Comparison of acquired diffusion weighted imaging and computed diffusion weighted imaging for detection of hepatic metastases.

Hironori Shimizu, MD, Hiroyoshi Isoda, PhD, MD, Koji Fujimoto, PhD, MD, Seiya Kawahara, MD, Akihiro Furuta, MD, Toshiya Shibata, PhD, MD, Kaori Togashi, PhD, MD

Department of Diagnostic Imaging and Nuclear Medicine, Kyoto University Graduate School of Medicine.

Address correspondence to: Hironori Shimizu, MD.

Department of Diagnostic Imaging and Nuclear Medicine, Kyoto University Graduate School of Medicine, 54 Kawahara-cho, Shogoin, Sakyo-ku, Kyoto 606–8507, Japan. Tel.: 81-75-751-3760 Fax: 81-75-771-9709

E-mail: hshimizu@kuhp.kyoto-u.ac.jp

The other authors:

Hiroyoshi Isoda, MD, PhD. E-mail: sayuki@kuhp.kyoto-u.ac.jp

Koji Fujimoto, MD, PhD. E-mail: kfb@kuhp.kyoto-u.ac.jp

Seiya Kawahara, MD. E-mail: butaemon@kuhp.kyoto-u.ac.jp

Akihiro Furuta, MD. E-mail: akihirof@kuhp.kyoto-u.ac.jp

Toshiya Shibata, MD, PhD. E-mail: ksj@kuhp.kyoto-u.ac.jp

Kaori Togashi, MD, PhD. E-mail: ktogashi@kuhp.kyoto-u.ac.jp

Their address and numbers of telephone and FAX are same as indicated above.

Objective: To compare the accuracy of acquired diffusion weighted imaging (DWI) (b=1000 sec/mm^2) with that of computed DWI (b=1000 sec/mm^2) for the detection of hepatic metastases. **Methods**: Two hundred and sixty patients underwent abdominal magnetic resonance imaging (MRI) at 3.0T for the evaluation of hepatic metastasis, including T1-weighted imaging (T1WI), T2-weighted imaging (T2WI), heavily T2WI, DWI with b-values of 0, 500, 1000 sec/mm^2, and three-dimensional dynamic contrast-enhanced MRI with gadolinium-ethoxybenzyl-diethylenetriamine pentaacetic acid (Gd-EOB-DTPA), and 190 patients were included in the final study. Computed DWI (=1000 sec/mm^2) was synthesized from lower b-values (b=0 and 500 sec/mm^2). Two groups were assigned and compared: group A (acquired DWI) and group B (computed DWI). Diagnostic performance using each imaging set was evaluated by receiver operating characteristic (ROC) curve analysis. **Results**: A total of 76 hepatic metastases were confirmed. The area under the ROC curve (Az) of group A was larger than that of group B (Observer 1; 0.919 to 0.915, Observer 2; 0.926 to 0.901), but there were no significant differences (observer 1, P = 0.500; observer 2, P = 0.190). There were 5 metastases visualized in group A, but these were difficult to detect in group B. However, there were 2 metastases that were better visualised in group B than in group A. **Conclusion**: There were no significant differences between acquired DWI and computed DWI in the detection of hepatic metastasis.

Keywords:

Magnetic Resonance Imaging; Diffusion MRI; Computed DWI; Hepatic metastasis

Introduction

Diffusion weighted imaging (DWI) has a potential role to play in the differentiation and evaluation of liver tumors on the basis of a high contrast between lesion and normal tissue. DWI can help direct the attention of the radiologist to findings that may otherwise be overlooked [1]. Shimada et al. reported that gadolinium-ethoxybenzyl-diethylenetriamine pentaacetic acid (Gd-EOB-DTPA) enhanced magnetic resonance imaging (MRI) showed higher accuracy in the detection of small metastases than DWI, but the addition of DWI was useful [2]. The sensitivity of a DWI sequence is characterized by its b-value. A higher diffusion weighting or b-value setting is desired to achieve higher contrast between normal liver parenchyma and solid lesions. Images of higher b-values give diffusion information that helps focal liver lesion characterization, and are sensitive in detecting lesions of higher cellular density [3,4]. However, higher b-value settings can cause severe image distortions and the use of longer TE reduces the signal-to-noise ratio (SNR) resulting in poorer image resolution. Thus, the optimal b-value should be determined based on the purpose of the examination [3]. The apparent diffusion coefficient (ADC) of each voxel can be calculated automatically by current MR systems by assuming a mono-exponential model of signal decay between two or more b values as follows:

$$\mathrm{ADC} = -\frac{ln\left(\frac{S_1}{S_0}\right)}{b_1 - b_0}$$

, where S_0 is signal intensity for $b = b_0$ and S_1 is that for $b = b_1$. ADC distribution

is illustrated on an axial ADC map. Once ADC is known, signal intensities for each voxel of higher b-value (or any b-value) images can be calculated as follows:

$$S_b = S_0 \cdot e^{-(b-b_0)\cdot ADC} = S_1 \cdot e^{-(b-b_1)\cdot ADC}$$

In this study, we used lower b-values (=0, 500 sec/mm^2) for imaging and then computed higher b-value (=1000 sec/mm^2) images using estimated ADC values with a mono-exponential model. The purpose of our study was to use receiver operating characteristic (ROC) analysis to retrospectively compare the accuracy of acquired DWI (b=1000 sec/mm^2) with that of computed DWI (b=1000 sec/mm^2) for the detection of hepatic metastases.

Materials and methods

Patients

Two hundred and sixty patients underwent Gd-EOB-DTPA-enhanced MRI for evaluation of hepatic metastasis at the Department of Radiology, Kyoto University Graduate School of Medicine, Kyoto, Japan, from July 2008 to September 2010. This study was performed in accordance with the Declaration of Helsinki. Local ethics committee approval was granted, and written informed consent was obtained from all patients. Informed consent for imaging examinations was obtained from all patients. Of the 260 patients, 53 patients were excluded from the study because they had neither histological proof nor follow-up confirmation. To minimize bias, 17 additional patients found to have more than 6 focal hepatic lesions also were excluded. 190 other patients (including 116 men and 74 women, aged 36-87 years, mean age 64.9 years) were included in the final study.

Lesion confirmation

The presence or absence of hepatic metastases was decided in consensus by two radiologists (S.K. and T.S., with 7 and 28 years' experience, respectively, in gastrointestinal and hepatobiliary imaging) who were not the two blinded readers who performed image analysis. The two radiologists determined the presence or

absence of metastases on the basis of findings obtained with contrast-enhanced computed tomography (CT), ultrasonography (US), positron emission tomography (PET) using F-18 fluorodeoxyglucose (FDG), and MRI; findings obtained in a follow-up CT and MRI; and findings obtained at definitive surgery that involved intraoperative US and serological examination. Twenty-six patients underwent definitive surgery with intraoperative US within 30 days of MRI, and 47 hepatic metastases were confirmed histologically in these patients. The 29 visible hepatic tumors in 12 patients for whom histopathological confirmation of disease was not available were considered to be hepatic metastases on the basis of tumor growth observed at follow-up examinations (performed 3-16 months after MRI). Tumor growth was defined according to the Response Evaluation Criteria in Solid Tumors (RECIST). There were no patients with hepatic cirrhosis in this study. As a final result, 76 hepatic metastases (size range, 0.4–4.5 cm; mean, 1.4 cm) in 38 patients (including 24 men and 14 women, aged 36-87 years, mean age 63.3 years) were confirmed, and 152 patients had no metastases (Table 1). Of the 38 patients, 20 patients had solitary lesions, 8 patients had two lesions, 2 patients had three lesions, 6 patients had four lesions, and 2 patients had five lesions. Primary cancer sites in each patient were as follows: 24 colorectal cancers, 10 pancreatic cancers, one common bile duct cancer, one gallbladder cancer, one lung cancer, and one esophageal cancer.

Imaging protocols

All MRI examinations were performed at 3.0 T using a commercially available MR system (Magnetom Trio Tim; Siemens Medical Solutions, Erlangen, Germany) equipped with spine matrix coil and body matrix coil. Baseline MR images, including a fat-saturated T2-weighted MR imaging (T2WI) turbo spin-echo (TSE) sequence with respiration triggering using a prospective acquisition correction (PACE) method, a breath-hold heavily T2WI with half-Fourier single-shot turbo spin-echo (HASTE) sequence and a breath-hold T1-weighted imaging (T1WI) gradient-echo (GRE) sequence with dual-echo of in- and opposed-phases were acquired before the administration of Gd-EOB-DTPA. Dynamic and delayed hepatocyte phase T1-weighted three-dimensional (3D) spoiled GRE images in the axial plane were obtained using a volumetric interpolated breath-hold examination (VIBE) sequence with chemically selective fat saturation. Images with the initial VIBE sequence were acquired before administration of contrast agent. A bolus of 25 μmol/kg body weight Gd-EOB-DTPA (Bayer Schering Pharma AG, Berlin, Germany) was injected and flushed with 40 ml of sterile saline solution at a rate of 2.5 ml/s from the antecubital vein. A power injector (Sonic Shot, Nemoto-Kyorindo, Tokyo, Japan) was used for injection of contrast agent and saline. Three dynamic phases, arterial (delay time 25 seconds), portal venous (65 seconds), and equilibrium (110 seconds) phases were acquired after a bolus injection of Gd-EOB-DTPA with fixed delay. After the dynamic study, images were obtained with a T1-weighted VIBE sequence in the hepatocyte phase at 20–25 min after injection of contrast agent. DWI using a single-shot spin-echo (SE) echo-planar

imaging (EPI) sequence in the axial plane with respiration triggering using the PACE method was acquired between the dynamic phase and the hepatocyte phase. The imaging parameters of all sequences are summarized in Table 2.

Imaging analysis

The same two radiologists who confirmed 76 hepatic metastases selected the anatomic section levels passing around the center of lesions on DWI. Among the section levels, 8 each had two metastases. Thus, the number of section levels with positive signals was 68 (60 Section levels each with one tumor and 8 section levels each with two tumors). A total of 76 section levels without metastases were randomly selected from the remaining section levels. Consequently, 144 section levels were selected for analysis. A total of 11 benign lesions, which were consistent with 10 cysts and a hemangioma, were also identified in the selected section levels. Diagnosis of cyst was determined by means of typical findings at US, T2WI, heavily T2WI and contrast-enhanced CT or MRI [5, 6]. Diagnosis of hemangioma was determined by means of findings of typical enhancement pattern at dynamic contrast-enhanced CT or MRI, typical high signal intensity on T2WI and heavily T2WI, and the fact that the lesions demonstrated no change in size during serial imaging studies for 3 months or more (3–16 months) [7, 8]. Two image groups were assigned and compared: group A (acquired DWI) and group B (computed DWI). Two readers (H.S. and H.I. with 7 and 22 years' experience, respectively, in gastrointestinal and

hepatobiliary imaging) interpreted images independently. These two readers were not the two radiologists who had determined the presence or absence of tumors on the basis of radiological and pathological findings. They knew that the patients were at risk of hepatic metastases but were blinded to all other information about the patients' history, including the site of primary tumor. They were not told how many hepatic lesions were in each section level. The diagnostic performance of each group for all hepatic metastases was evaluated by each observer using receiver operating characteristic (ROC) curve analysis. To minimize any learning bias, we randomized the order of the section levels before every session and scheduled a two-week interval between the two interpretation sessions. Each observer recorded the presence and segmental location of lesions, assigning each a confidence level on a 5-point scale: 1 = definitely not present; 2 = probably not present; 3 = equivocal; 4 = probably present; and 5 = definitely present. Sensitivity calculations were based on only those lesions awarded a confidence rating of 4 or 5. If they determined that there were multiple lesions in one section level, each suspected nodule was scored. A third radiologist (K.F. with 11 years' experience) correlated scored lesions with the reference standard on the basis of the description regarding lesion size and location as a coordinator.

Statistical analysis

For each imaging set, ROC curve analysis was performed using a maximum

likelihood estimation program (ROCKIT, version 1.0.1 B2; C. E. Metz, University of Chicago, Chicago, IL, USA). The diagnostic accuracy of each imaging set for each observer was calculated by measuring the area under the ROC curve (Az). Differences between imaging sets in terms of the mean Az values were analysed with the two-tailed Student's t test for paired data. The interobserver agreement for the evaluation of the two imaging sets was analysed with the kappa statistic. The agreement in terms of kappa values was as follows: <0.20 = poor agreement; 0.21-0.40 = fair agreement; 0.41-0.60 = moderate agreement; 0.61-0.80 = good agreement; and 0.81-1.00 = excellent agreement. The sensitivity and specificity for each image set were then calculated. The sensitivity and specificity of the two imaging sets were compared using McNemar's test. A two-tailed *P* value of less than 0.05 was considered to indicate a significant difference. Statistical analyses were performed using statistical software (SPSS, version 15.0; SPSS, Chicago, IL, USA).

Results

ROC curve analysis

For all 76 lesions, calculated Az values for each observer in group A (acquired DWI) and group B (computed DWI) are shown in Table 3. Az values for both observers were higher in group A than in group B, but there were no significant differences (observer 1, P = 0.500; observer 2, P = 0.190). Interobserver agreement was good for both group A and group B (group A, Kappa value = 0.702; group B, Kappa value = 0.723).

Sensitivity and specificity

The sensitivity and specificity from each observer for each image set for the detection of lesions are summarised in Table 4. Overall, there was higher sensitivity for group A than for group B. Specificity did not show a specific tendency. However, there were no significant differences between the two image sets for the two observers. Among the 76 lesions, there were five lesions that were clearly visualized on acquired DWI, but were difficult to detect on computed DWI. On the other hand, there were two metastases that were better visualised on computed DWI than on acquired DWI. For two observers, four false-positive lesions (three cysts and a hemangioma) were found in both group A and group B. There were four other false-positive lesions which either of the two readers

found in group A, and three lesions in group B.

Discussion

The accurate detection of hepatic metastases, especially small hepatic metastases, is clinically important because it may significantly affect the choice of therapeutic approach in many cases [9]. MRI, especially single-shot EPI DWI, can obtain high lesion-to-liver contrast even without contrast agent. Recently, abdominal DWI has become widely used for oncology patients because it can provide additional information in lesion detection, especially in the detection of hepatic metastasis [10, 11].

Computed DWI is a mathematical computation technique that builds on previously described principles, which calculates a high b-value (or any b-value) image for DWI acquired with at least two different b-values. In this way, disadvantages associated with direct high b-value measurements, such as poor SNR and image distortion, may be avoided [12]. In this study, we compared the accuracy of acquired DWI with that of computed DWI for the detection of hepatic metastases, which has not yet been performed. Accurate detection of hepatic metastases was achieved in both group A (acquired DWI) and group B (computed DWI) (Fig. 1). ROC curve analysis showed that the diagnostic performance of group A was better than that of group B for detecting hepatic metastases (Observer 1; Az = 0.919 to 0.915, Observer 2; Az = 0.926 to 0.901), but there were no significant differences (observer 1, $P = 0.500$; observer 2, $P = 0.190$). Regarding sensitivity and specificity, there were no significant differences. In some previous studies, the sensitivity of DWI was about 0.8-0.9 [2,10,11]. The sensitivity of our acquired DWI and computed DWI is comparable

to these studies. Based on these results, computed DWI may be useful when acquired higher b-value DWI is of poor quality.

There were two metastases that were better visualised on computed DWI than on acquired DWI. Simulation and computation of the diffusion properties of water molecules in each imaging voxel using a mono-exponential model is easy to understand, but the phenomenon that occurs in the human body is not so simple. The ADC value is sensitive not only to tissue diffusivity, but also to microcirculation of blood within normal capillary networks, which is also called perfusion. The influence of perfusion is significant especially in low b-values (less than 150-200 sec/mm^2), and a bi-exponential behavior has been observed in liver [13,14]. In 1986, Le Bihan D, et al proposed the term intravoxel incoherent motion (IVIM) that designates the microscopic translational motions that occur in each image voxel in MRI [15,16]. In this study, we use a mono-exponential model including a b=0 image greatly affected by perfusion. So ADC, the slope of the line formed by the measured two signal intensities in the logarithmic scale, is calculated to be lower than the actual value. Consequently, the signal intensity of tissues with blood flow is lower on computed DWI than on acquired DWI. This phenomenon is very important in the evaluation of normal liver and hepatic metastases. Koh et al. reported that the signal intensity curve for hepatic metastases on DWI is relatively flat at low b-values, and this observation is in keeping with known pathology of hepatic metastases, which are usually hypovascular compared with normal liver parenchyma [13,17]. To summarize the above, the degree that ADC is to be calculated lower than the actual value is more serious in normal liver parenchyma, which is relatively

hypervascular than in hepatic metastasis. Thus, lesion-to-liver contrast on computed DWI is likely to be greater than that on acquired DWI (Fig. 2). On the other hand, there were five lesions that were clearly visualized on acquired DWI, but were difficult to detect on computed DWI. In one case, a small lesion close to hepatic vessels was difficult to detect on computed DWI (Fig. 3). Signal intensities of the heart and comparatively thick blood vessels, including an early blood flow, are calculated to be very low because the influence of perfusion is great. These structures are non-signal areas in a gray scale image (Fig. 4). Because of the influence of this error, it may become more difficult on computed DWI to detect the signal of small hepatic metastases that are very close to hepatic vessels including such an early blood flow. In addition to this case, there were four other lesions (three in the upper edge of the liver, the remaining one in the lateral segment) that were difficult to detect on computed DWI. Koh et al. reported that in phantom studies it is shown that for high b-values (> 840 sec/mm^2), SNR of computed DWI is improved compared with acquired DWI [12]. But in our study, there was a subtle shift in position between two piled images (b=0, 500 sec/mm^2) caused by physiological movement, so the influence of misregistration was more significant. Of the 76 hepatic metastases, 34 lesions were less than 1cm. These small lesions may be greatly affected by misregistration. It is difficult to detect small hepatic metastases especially in the upper edge and the lateral segment of the liver. There were four false-positive lesions in group A which were not found in group B. In these cases, image distortion caused by higher b-value settings may be avoided in computed higher b-value images using lower b-value images. There were three false-positive

lesions only found in group B, and the influence of misregistration is suspected.

Our study had several limitations. First, not all lesions were compared and confirmed with surgical specimens. Second, 17 patients found to have more than 6 focal hepatic lesions were excluded. Relatively many patients were excluded, and this might be leading to potential selection bias. Third, image selection in this study was not intentional, but bias may decrease the reliability of this study. Fourth, the 2-week interval between the two image interpretation sessions might not have been long enough to minimize learning bias. Fifth, we used a mono-exponential model and calculated ADC by two b-values. Mono exponential diffusion is contaminated by microperfusion, so a bi-exponential model should be used to capture information of both perfusion and molecular diffusion [18]. Currently, the clinical use of DWI is mainly based on ADC, so we used a mono-exponential model. To reduce the effect of noise, calculation of ADC should be performed using more than two b-values [19]. Though we could estimate ADC by using three b-values (0, 500, 1000 sec/mm^2), we estimated ADC by using two b-values except 1000 sec/mm^2 because we wanted to examine the usefulness of the computed DWI when the higher b-value acquired DWI is of poor quality. Sixth, DWI was acquired after the administration of Gd-EOB-DTPA to shorten the examination time, and this may have some effects on ADC values. However, a recent paper reported that ADCs of focal hepatic lesions were not significantly different before and after administration of contrast agent and that DWI after Gd-EOB-DTPA administration can be used as a substitute for unenhanced DWI at 3.0 T without compromising CNR and ADC of focal hepatic lesions [20].

Conclusions

There were no significant differences between acquired DWI and computed DWI in the detection of hepatic metastases. Although there is a problem in actually using computed DWI as a perfect substitute for acquired DWI, computed DWI may be useful when acquired higher b-value DWI is of poor quality.

Reference list

1. Kele PG, van der Jagt EJ. (2010) Diffusion weighted imaging in the liver. World J Gastroenterol. 16:1567-76

2. Shimada K, Isoda H, Hirokawa Y, Arizono S, Shibata T, Togashi K. (2010) Comparison of gadolinium-EOB-DTPA-enhanced and diffusion-weighted liver MRI for detection of small hepatic metastases. Eur Radiol. 20:2690-8

3. Nagakawa S, Kawai H, Fukatsu H, et al (2005) Diffusion-weighted Imaging of the Liver: Technical Challenges and Prospects for the Future. Magnetic Resonance in Medical Sciences

4. Taouli B, Koh DM (2010) Diffusion-weighted MR imaging of the liver. Ragiology

5. Mathieu D, Vilgrain V, Mahfouz A, et al (1997) Benign liver tumors. Magn Reson Imaging Clin N Am 5:255–288.

6. Mortele KJ, Ros PR (2001) Cystic focal liver lesions in the adult: differential CT and MR imaging features. Radiographics 21:895–910.

7. Horton KM, Bluemke DA, Hruban RH, et al (1999) CT and MR imaging of benign hepatic and biliary tumors. Radiographics 19:431–451.

8. Kim T, Federle MP, Baron RL, et al (2001) Discrimination of small hepatic hemangiomas from hypervascular malignant tumors smaller than 3 cm with three-phase helical CT. Radiology 219:699–706.

9. Zech CJ, Herrmann KA, Reiser MF, et al (2007) MR imaging in patients with suspected liver metastases: value of liver-specific contrast agent Gd-EOB-DTPA. Magn Reson Med Sci 6:43-52.

10. Nasu K, Kuroki Y, Nawano S, et al (2006) Hepatic metastases: diffusion-weighted sensitivity-encoding versus SPIO-enhanced MR imaging. Radiology 239:122-30.

11. Bruegel M, Gaa J, Waldt S et al (2008) Diagnosis of hepatic metastasis: comparison of respiration-triggered diffusion-weighted echo-planar MRI and five t2-weighted turbo spin-echo sequences. AJR 191:1421-9

12. Blackledge MD, Leach MO, Collins DJ, Koh DM. (2011) Computed Diffusion-weighted MR Imaging May Improve Tumor Detection. Radiology 261:573-81

13. Koh DM, Collins DJ, Orton MR. (2011) Intravoxel incoherent motion in body diffusion-weighted MRI:reality and challenges. AJR 196:1351-61

14. Koh DM, Collins DJ. (2007) Diffusion-weighted MRI in the body: application and challenges in oncology. AJR 188:1622-35

15. Le Bihan D, Breton E, Lallemand D, Grenier P, Cabanis E, Laval-Jeantet M. (1986) MR imaging of intravoxel incoherent motions: application to diffusion and perfusion in neurologic disorders. Radiology 161:401-7

16. Le Bihan D, Breton E, Lallemand D, Aubin ML, Vignaud J, Laval-Jeantet M. (1988) Separation of diffusion and perfusion in intravoxel incoherent motion MR imaging. Radiology 168:497-505

17. Koh DM, Scurr E, Collins DJ, et al (2006) Colorectal hepatic metastases:quantitative measurements using single-shot echo-planar diffusion-weighted MR imaging. Eur Radiol 16;1898-905

18. Hildebrand Dijkstra, Paul Baron, Peter Kappert, Matthijs Oudkerk, Paul E. Sijens (2012) Effects of microperfusion in hepatic diffusion weighted imaging.

Eur Radiol 22:891-9

19. Boris Guiu, Jean-Pierre Cercueil (2011) Liver diffusion-weighted MR imaging: the tower of Babel? Eur Radiol 21:463-7

20. Choi JS, Kim MJ, Choi JY, Park MS, Lim JS, Kim KW (2010) Diffusion-weighted MR imaging of liver on 3.0-Tesla system: effect of intravenous administration of gadoxetic acid disodium. Eur Radiol 20:1052-60

Figure Legends

Fig. 1: Surgically proven hepatic metastases from colon cancer in a 54-year-old man. (a) Acquired DWI shows two metastases at S4/8 and S1 (arrow). (b) These lesions are also clearly visualised on computed DWI (arrow).

Fig. 2: Surgically proven hepatic metastasis from colon cancer in a 65-year-old man. (a) Small hepatic metastasis at the periphery of S7/8 is obscurely visualised on acquired DWI (arrow). The signal intensity of this lesion is 20.8 (arbitrary unit; a.u.), and that of normal liver parenchyma is 13.6 (a.u.). (b) The same lesion is more clearly visualized on computed DWI (arrow). The signal intensity of this lesion on computed DWI is 21.0 (a.u.), which is almost the same to on acquired DWI. The signal intensity of normal parenchyma on computed DWI is 7.7 (a.u.), which is lower than on acquired DWI. As a result, lesion-to-liver contrast is greater.

Fig. 3: Hepatic metastasis from pancreatic cancer in a 57-year-old man. (a)Small hepatic metastasis in S6 is visualized on acquired DWI (arrow). (b) On computed DWI, it is difficult to detect this lesion. (c) On the portal venous phase of dynamic contrast-enhanced MR imaging with Gd-EOB-DTPA, this small metastasis is shown as a small low signal intensity area that is very close to hepatic vessels (arrow).These hepatic vessels are non-signal on computed DWI, so the signal intensity of adjacent small hepatic metastasis may be influenced by this error.

Fig. 4: Hepatic metastasis from pancreatic cancer in a 46-year-old man. (a) Acquired DWI shows small metastasis at the upper edge of right lobe of the liver (arrow). (b) Computed DWI shows this lesion clearly (arrow). The heart and the Aorta represent non-signal areas (arrowhead). These structures, including an early blood flow, are calculated to be very low because the influence of perfusion is great.

Table 1

The Number of Patients and Detected Lesions

	Number of patients	Number of lesions
Patients with histologically proven hepatic metastases	26	47
Patients with hepatic metastases confirmed by follow-up study	12	29
Patients without hepatic metastases	152	0

Table 2
MR imaging parameters

	T2WI	heavily T2WI	T1WI (dual echo)	3D VIBE dynamic contrast	DWI
TE	71 ms	145 ms	in 2.46 ms out 1.26 ms	1.07 ms	71 ms
TR			200 ms	3 ms	
ETL	18	175			96
ETS	7.08 ms	5.78 ms			0.57 ms
slice thickness	5 mm	5 mm	5 mm	3 mm	5 mm
gap between slices	1 mm	1 mm	1 mm	no gap	1 mm
flip angle	120°	150°	60°	10°	
matrix size	256×256	175×320	147×256	154×256	96×128
FOV	36 cm	36 cm	36 cm	36 cm	36 cm
number of slices	30	30	30	60	30
GRAPPA factor	2	2	2	2	2
acquisition time		20×2 sec during two breath-holds at end-expiration	17 sec	16 sec	
				number of signals acquired = 1	b factors = 0, 500, 1000 sec/mm^2

TE, echo time; TR, repetition time; ETL, echo train length; ETS, echo train spacing; FOV, field of view; GRAPPA, generalized auto calibrating partiall

Table 3

Area Under the Receiver Operating Characteristic Curve (Az) and *P* Values of Group A (acquired DWI) and Group B (computed DWI) in the Detection of Hepatic Metastases

Area under ROC curve (Az) imaging sets	Observer 1	Observer 2	Kappa value
Group A	0.919	0.926	0.702
Group B	0.915	0.901	0.723
P value	0.500*	0.190*	

*The difference between the two imaging sets is not significant.

Table 4

Sensitivity and Specificity of Group A (acquired DWI) and Group B (computed DWI)

Imaging sets	Observer 1	Observer 2
Sensitivity (%)		
Group A	86.84	86.84
Group B	81.58	78.95
P value	0.221*	0.077*
Specificity (%)		
Group A	92.11	90.79
Group B	90.79	93.42
P value	1.000*	0.617*

*The difference between the two imaging sets is not significant.

Fig.1a

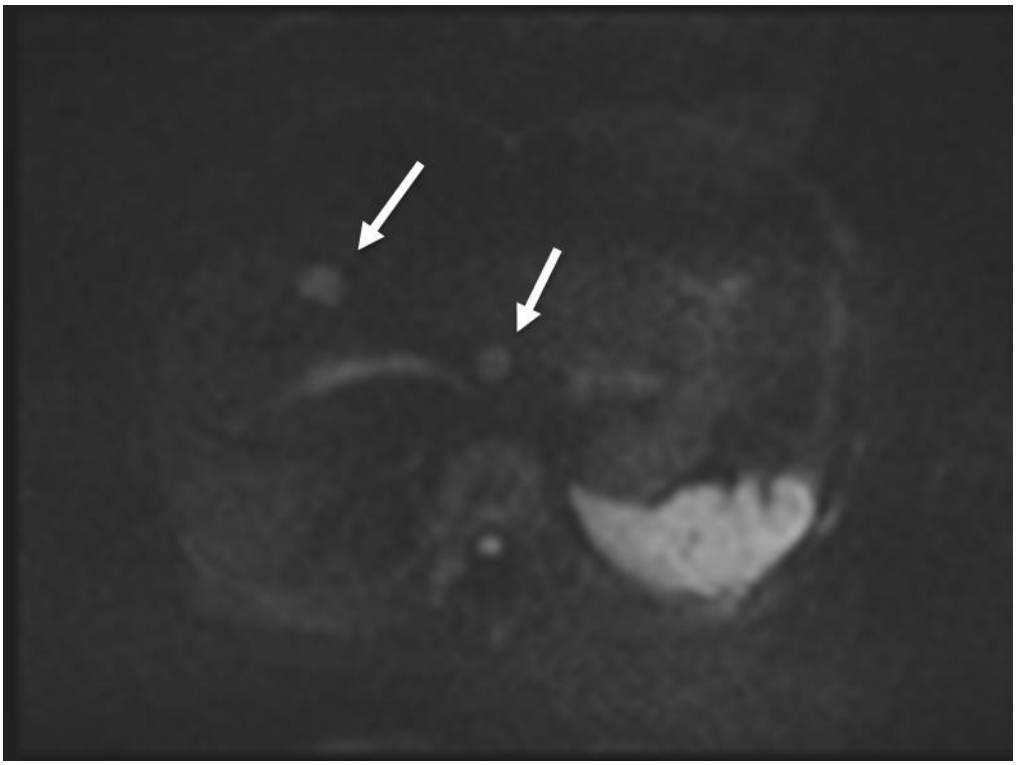

Fig.1b

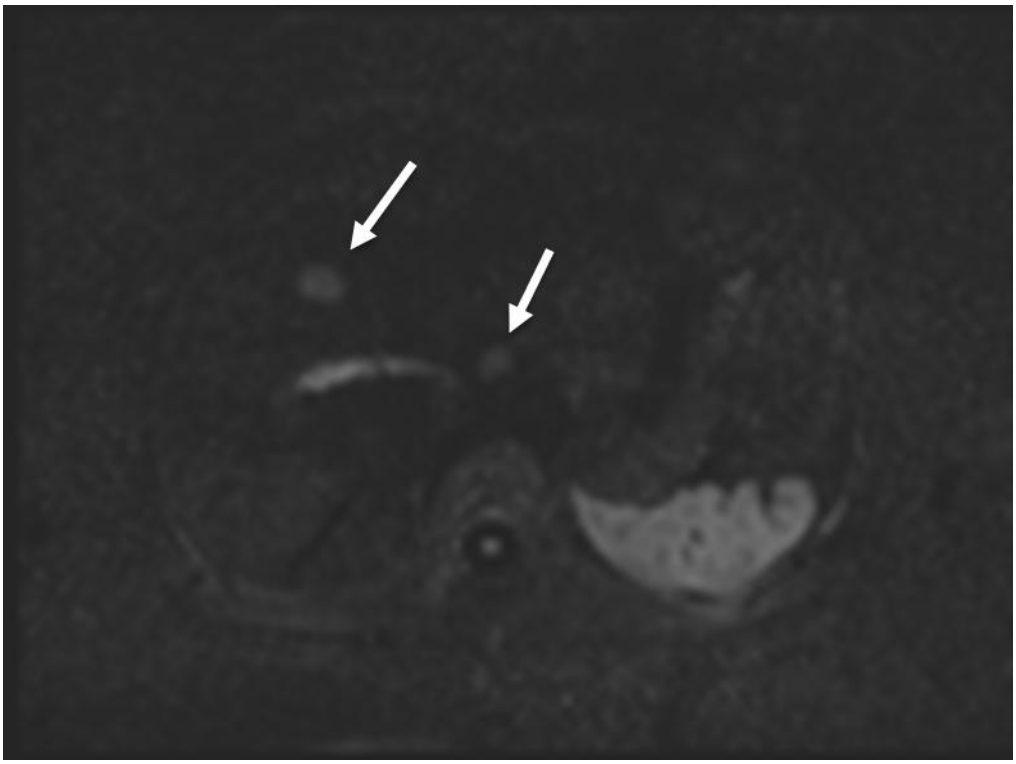

Fig.2a

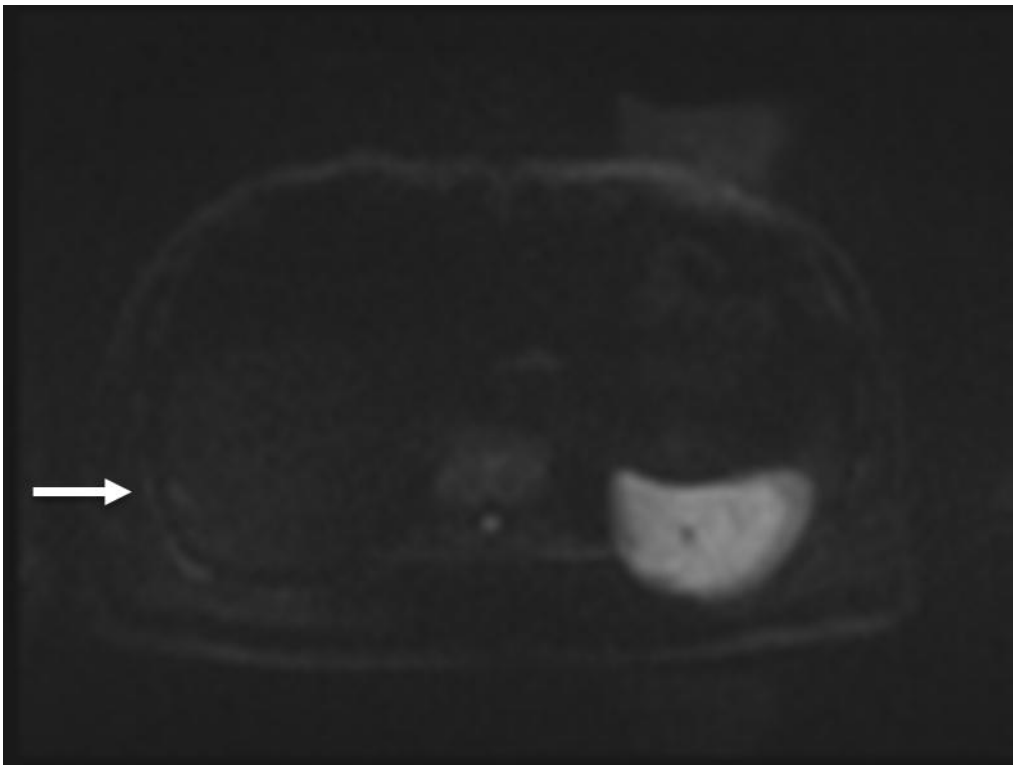

Fig.2b

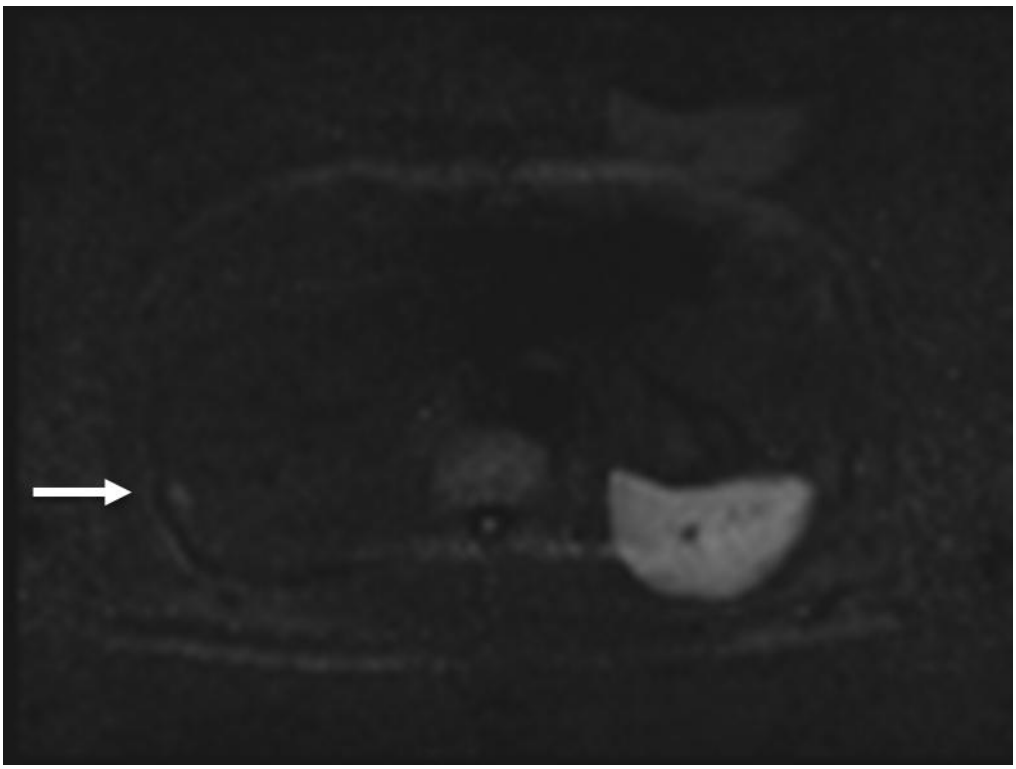

Fig.3a

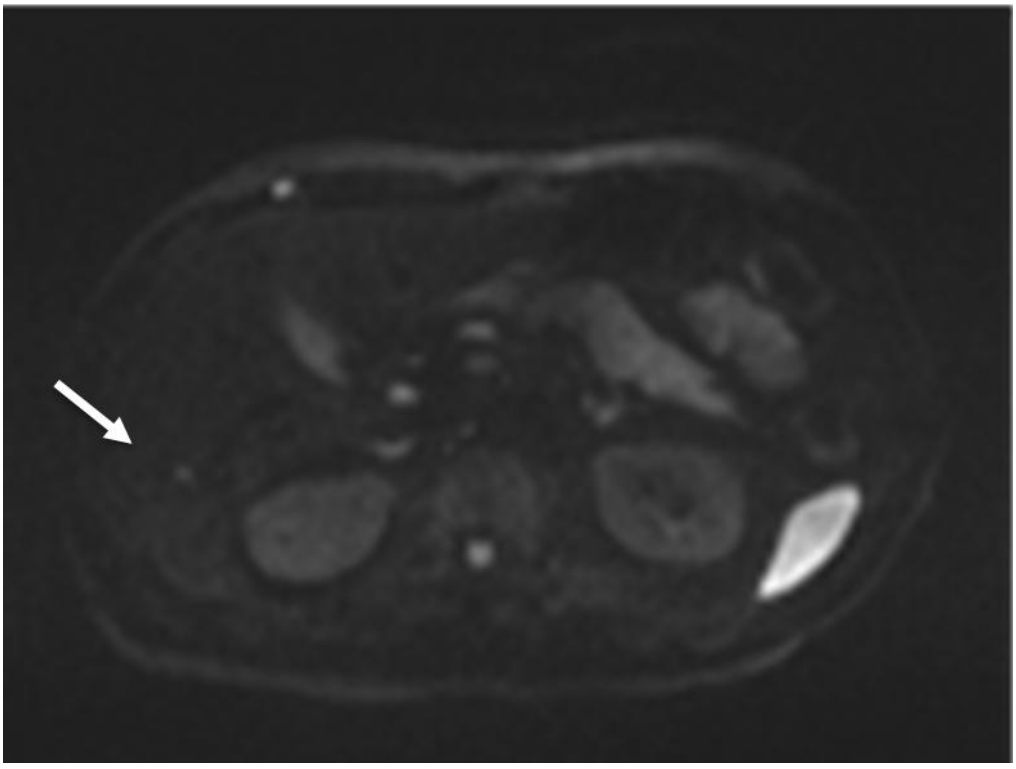

Fig.3b

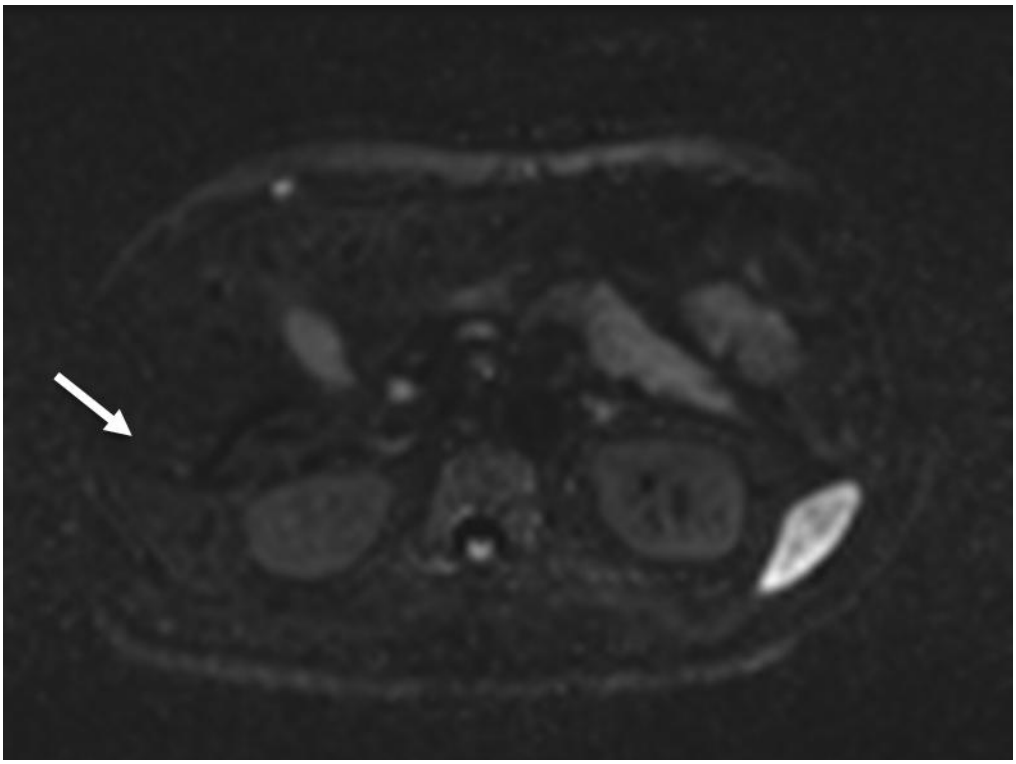

Fig.3c

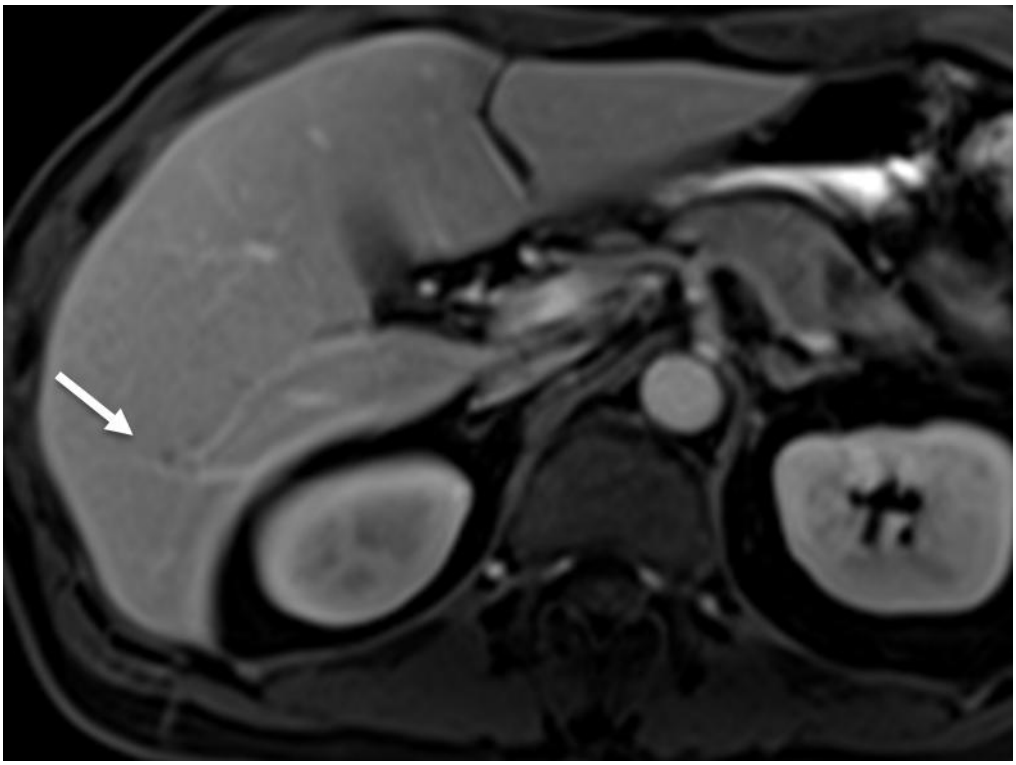

Fig.4a

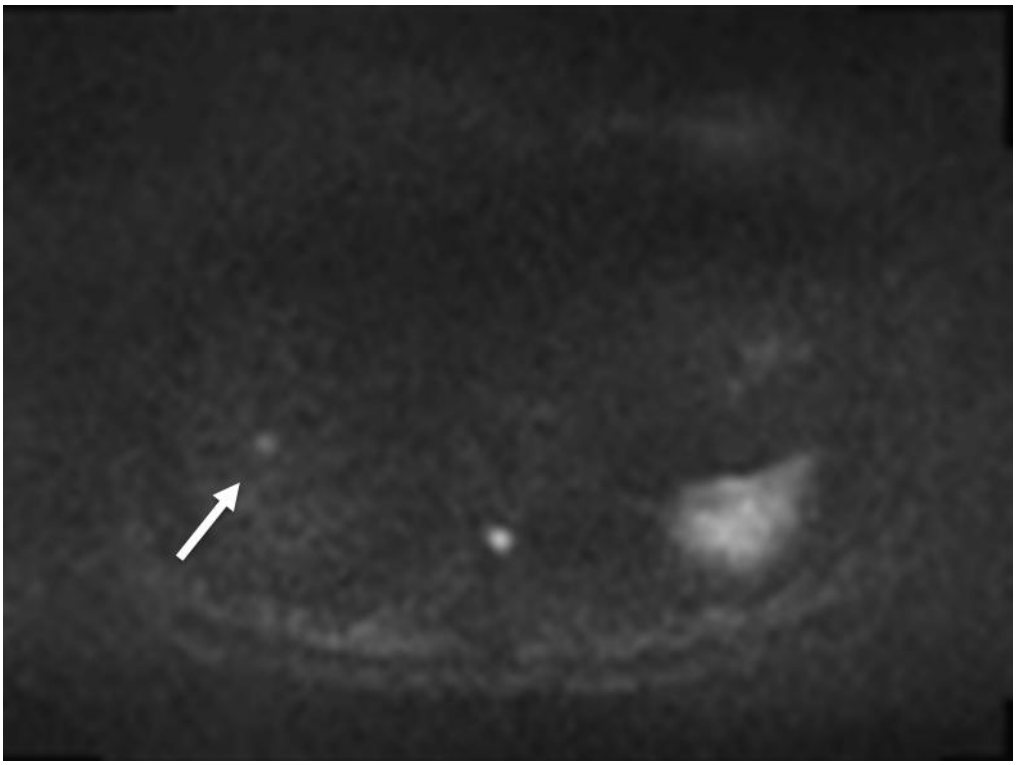

Fig.4b